Experimental study on the fundamental frequency of prestressed concrete bridge beams with parabolic unbonded tendons

M. Bonopera[a,d*], K.C. Chang[b], C.C. Chen[a], Y.C. Sung[c], N. Tullini[d]

[a]Bridge Engineering Division, National Center for Research on Earthquake Engineering
No. 200, Sec. 3, Xinhai Road, Taipei, 10668, Taiwan

[b]Department of Civil Engineering, National Taiwan University
No. 1, Sec. 4, Roosevelt Road, Taipei, 10617, Taiwan

[c]Department of Civil Engineering, National Taipei University of Technology
No. 1, Sec. 3, Zhongxiao E. Road, Taipei, 10608, Taiwan

[d]Department of Engineering, University of Ferrara
No. 1, Via Saragat, Block A, Ferrara, 44122, Italy

*Corresponding author - Emails: bonopera@ncree.narl.org.tw - marco.bonopera@unife.it

Abstract

In this study, a laboratory experiment–based testing program was conducted on a large-scale high-strength Prestressed Concrete I (PCI) beam with a parabolic unbonded tendon, capable of simulating a typical prestressed bridge member. Specifically, the simply supported PCI beam was subjected to free transverse vibrations with different prestress forces to demonstrate that its fundamental frequency was unaffected by such force. A reference model, describing the behavior of the PCI beam as a combination of two substructures interconnected, i.e., a compressed concrete Euler–Bernoulli beam and a tensioned parabolic cable, predicts no change in fundamental frequency with increasing prestress force when variation of the concrete's initial elastic modulus over time is taken into account. The large-scale experimental results confirmed that fundamental frequency is not an appropriate parameter for prestress loss prediction in concrete bridge beams with parabolic unbonded tendons. Accordingly, subsequent studies will be conducted for improving a static nondestructive testing method for such detection in concrete bridges.

Keywords: concrete bridge beam; elastic modulus; fundamental frequency; prestress loss; parabolic unbonded tendon

1. Introduction

The natural frequency of prestressed concrete beams is a crucial parameter in defining the dynamic behavior of a bridge. Whether the dynamic response of prestressed beams is affected by applied prestress force has been discussed extensively (e.g., in the literature review by Noble et al. [1, 2]). Several studies [3–10] have assumed that prestress force in the tendon is equivalent to external axial force on each beam end. Consequently, the natural frequencies of prestressed members tend to decrease with increasing compressive force, which is termed the "*compression-softening*" effect. This effect occurs in externally axially loaded Euler–Bernoulli beams prone to buckling failure [6–12]. An experimental study also demonstrated this behavior in prestressed concrete beams with parabolic tendons [13]. Nonetheless, several dynamic tests have reported an increase in natural frequencies with increasing prestress force [14–18] as occurs in tension members within the elastic range [11, 12, 19–21], thus contradicting the "*compression-softening*" theory. Toyota et al. [22] observed the same behavior in a post-tensioned concrete beam with a bonded or unbonded tendon. More specifically, Saiidi et al. [15] noted that an increase in prestress force seemed to influence microcrack closure and thus increase the stiffness and natural frequencies of concrete beams [23–25]. Moreover, Noh et al. [26] suggested that the natural frequency of concrete members with parabolic unbonded tendons was also increased by other parameters, such as the beam camber, cable geometric stiffness, and stiffness effect of the beam–tendon system. By contrast, Bonopera et al. [9] proved experimentally that the fundamental frequency of concrete bridge members with straight tendons is unaffected by prestress force. Similarly, Hamed and Frostig [27] suggested, based on numerical results, that the natural frequencies of concrete beams with parabolic tendons remain unchanged by prestressing. They claimed that prestress force in the tendon modified its original line of action during member vibration, thereby preserving force eccentricity with respect to the beam axis. Accordingly, prestress force did not cause Euler buckling. Vice versa, an external compressive force retained its original line of action, varying the force eccentricity with respect to the beam axis during vibrational displacement. Given the discrepancies in these findings, it remains unclear which might represent a reference model for properly evaluating the dynamic behavior of prestressed concrete bridge beams with parabolic unbonded tendons. The aforementioned studies also lack experimental data on the relationship between prestress force and fundamental frequency in large-scale prestressed concrete members, because their experiments were conducted only on small-scale beams whose slenderness and stiffness rendered them unsuitable for simulating concrete bridge beams. Moreover, the mass of load cells and especially stressing jacks, at boundary ends, can influence the dynamic response of small-scale members [15–16, 28]. Dynamic testing on large-scale beams minimizes the effect of these masses, as verified by the numerical simulations of Bonopera et al. [9]. Proper information on the dynamic behavior of concrete members is also required for studying prestress loss phenomena [8–9, 29].

For these reasons, a large-scale simply supported Prestressed Concrete I (PCI) beam made of high-strength concrete with a parabolic unbonded tendon was used in this study. The beam was subjected to free transverse vibrations with different prestress forces on specific days, therefore simulating different concrete curing conditions. A set of servo velocity seismometers were installed along the PCI beam's span to measure the fundamental frequency. The model proposed by Song [30], describing the behavior of the simply supported PCI beam as a combination of two substructures interconnected, i.e., a compressed concrete Euler–Bernoulli beam and a tensioned parabolic cable, was the reference solution. The elastic modulus was obtained daily through compression tests on concrete cylinders. The results indicated that experimental fundamental frequencies could be simulated using the aforementioned solution, thus demonstrating that the beam mechanical model's assumption was accurate. Numerical examples are presented to illustrate the difference between fundamental frequencies determined by the model proposed by Song [30] and other models mentioned in the literature. The fundamental frequency of a concrete bridge beam with a parabolic unbonded tendon is unaffected by prestress force because small second-order effects were usually induced in these prestressed members. Furthermore, the frequency remained relatively constant over time, with variation of the initial concrete elastic modulus caused by the early curing process. The large-scale experimental results also confirmed that fundamental frequency is not an appropriate parameter for determining prestress loss in concrete members, as suggested in the literature [9, 15, 25]. In this regard, a static Non-Destructive Testing (NDT) method [8] based on the "*compression-softening*" theory seems more reliable than dynamic methods of prestress loss prediction in concrete beams with straight unbonded tendons. Consequently, future studies are planned for improving the aforementioned static method for such detection in concrete bridges.

2. Large-scale laboratory testing program

2.1 PCI beam with a parabolic unbonded tendon and related test layout

A large-scale PCI beam of width b = 450 mm and height h = 900 mm was adopted (Fig. 1). The beam was longitudinally reinforced with rebars and transversally with stirrups, in accordance with the Building Code Requirements for Structural Concrete [31], corresponding to a unit weight of steel ρ_s of approximately 1.23 kN/m^3. Two pinned-end supports were placed at the beam ends to reproduce the most common boundary conditions of prestressed concrete bridge beams, resulting in a clear span of L = 14.5 m (Fig. 1). The parabolic unbonded tendon had a small eccentricity e_1 of 120.5 mm (e_1 / h = 0.13) at the beam ends and a large eccentricity e_2 of 270 mm (e_2 / h = 0.30) at the midspan with respect to the centroid of the cross-section. Its deflected shape was $f = e_2 - e_1$ = 149.5 mm, whereas the corresponding ratio was f / L = 0.01. Specifically, the tendon was composed of 15 seven-wire strand steel cables that were 15.2 mm in diameter and inserted into 15 plastic ducts embedded along the concrete beam's length (Fig. 1). The plastic ducts were not injected. The ultimate yield strength and elastic modulus of the steel cables were σ_{uy} = 1860 MPa and E_{tendon} = 200 GPa, respectively. The cross-sectional second moment of the area of the PCI beam's section (concrete only) I_{concr} was 2.509 × 10^{10} mm^4, and the corresponding cross-sectional area A_{tot} was 2.982 × 10^5 mm^2. The slenderness ratio was 50, and the beam had a rectangular cross-section equal to b × h, that is, 450 × 900 mm^2, for a length of 650 mm from the pinned-end supports. The cross-sectional area of the parabolic tendon $A_{tot,tendon}$ was 2.085 × 10^3 mm^2, whereas its effective length was L_{tendon} = [1 + 8/3 × $(f / L)^2$] × L = 14.504 m [30]. All geometric dimensions were verified by measuring systems with 0.01-mm tolerance (laser rangefinder and caliper) after the member was positioned on the supports. The elastic modulus of the high-strength concrete was evaluated through compression tests on cylinders after 28 days of curing and during the experimental period (Section 2.3).

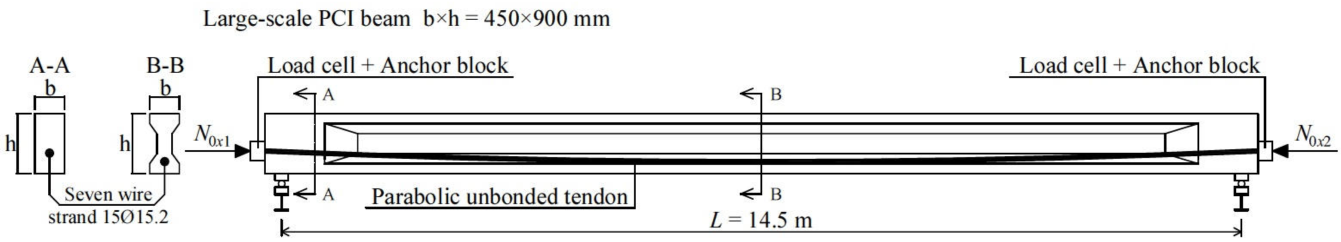

Fig. 1. Large-scale PCI beam with a parabolic unbonded tendon.

The PCI beam was inserted into a test rig (Fig. 2(a)). At one beam end, a hydraulic oil jack of 4000 kN force capacity was used to apply different prestress forces by pulling the parabolic tendon outward. A 4000 kN load cell with an accuracy of 2 mV/V was placed at either end to measure the assigned prestress forces N_{0x1} and N_{0x2} (Fig. 3(a)). Three prestress forces $N_{0x,\mathrm{aver}}$ were applied in values of approximately 1658, 1829, and 1952 kN to prevent cracking phenomena and induce small second-order effects as typical for concrete bridge beams [9, 32], equaling to 3.5%, 3.8%, and 4.1% of the PCI beam's buckling load N_{crE}, respectively. A difference of approximately 170 kN between the prestress forces $N_{0x,\mathrm{aver}}$ was initially planned. The laboratory's indoor safety conditions involved the higher prestress force $N_{0x,\mathrm{aver}}$ of 1952 kN. Thus, the maximum tensile strength in the tendon was of approximately 50% of the ultimate yield strength of the cables [9, 32]. The different prestress forces N_{0x1} and N_{0x2} measured at the beam ends were caused by friction losses along the tendon (Fig. 1). The measurement systems included four servo velocity seismometers and four Linear Variable Differential Transformers (LVDTs) deployed along the PCI beam's length (Fig. 4). The arrangement of these devices is described as follows:

Servo velocity seismometer: Four VSE–15D high-precision servo velocity seismometers, manufactured by Tokyo Sokushin Co., Ltd., were chosen for the experiments (Fig. 3(b)). The seismometers had a sensitivity of 5 mV/g and were lightweight (270 g). One seismometer, labeled A5, was placed vertically on the top of the PCI beam at a point corresponding to the midspan cross-section (i = 5) to collect acceleration data with respect to the strong axis (Fig. 4). Two seismometers, labeled A0 and A10, were placed at the beam ends (i = 0 and 10). One reference seismometer, labeled Af, was additionally fixed to the floor close to the beam end at i = 10 to record possible abnormalities of the sensing system. All sensors were connected to a signal conditioner and, subsequently, to a data logger located on a desk close to the test rig (Fig. 5(c)). The test layout in Fig. 4 shows their positions (in red).

LVDT: Two LVDTs with a tolerance of 0.002 mm, manufactured by Tokyo Sokki Kenkyujo Co., Ltd., were positioned on the opposite sides of the midspan cross-section at i = 5 (Fig. 4). Steel plates were used to position each LVDT probe at the level of the beam axis (Fig. 2(b)). Additionally, two reference LVDTs, labeled L0 and L10, were fixed at the beam ends i = 0 and 10, respectively, forming a reference line between the boundary conditions for the measurement system. All LVDTs were connected to a data logger positioned on a desk close to the test rig to acquire signals. The test layout in Fig. 4 shows their positions (in blue).

(a) **(b)**

Fig. 2. (a) Indoor test rig. (b) Transverse steel beam and one LVDT at the PCI beam's midspan.

(a) **(b)**

Fig. 3. (a) Load cell, steel transition part, and circular plate at one PCI beam end. (b) One servo velocity seismometer placed on the top of the PCI beam.

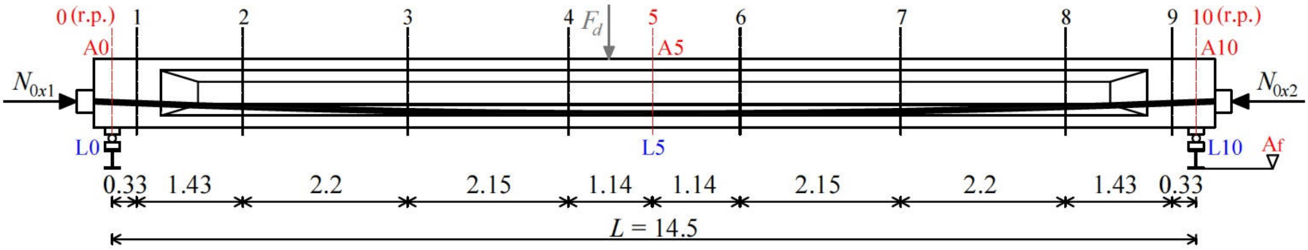

Fig. 4. Test layout with locations of instrumented sections with velocity seismometer and LVDT sensing systems. Units in meters.

2.2 Free vibration tests

Free vibration tests were performed following the application of prestress forces $N_{0x,\mathrm{aver}}$. Three test cases with $N_{0x,\mathrm{aver}}$ equal to 1658, 1829, and 1952 kN were examined. All the servo velocity seismometers acquired acceleration data using a sampling rate of 200 Hz and a block size of 32,768 samples (Fig. 5(c)). Vibration measurements were performed three times for each imposed prestress force $N_{0x,\mathrm{aver}}$ for a total of nine experiments. Specifically, free transverse vibrations were induced by breaking a steel rebar of 10 mm in diameter anchored close to the PCI beam's midspan (Fig. 5(a)). The rebar's ultimate strength f_{sk} of 540 MPa was achieved using a hydraulic oil jack of 100 kN force capacity, pulling each rebar up until rupture (Fig. 5(a)). The hydraulic oil jack was driven by a hydraulic pump of 96.53-MPa in maximum pressure capacity positioned to the floor (Fig. 5(b)). The large-scale PCI beam was thus vertically excited by a release force F_d of approximately 42.4 kN (Fig. 4), and its dynamic response was measured along its strong axis. The PCI beam did not develop any cracks during testing. The applied prestress forces N_{0x1} and N_{0x2} were recorded every second for exactly 200 seconds by a data acquisition unit using a different data logger. The cables under tensile forces were always in contact with the surrounding plastic ducts during testing.

(a) **(b)** **(c)**

Fig. 5. (a) Arrangement of the hydraulic oil jack on one steel rebar anchored close to the PCI beam's midspan. (b) Arrangement of the hydraulic pump on the floor before activation. (c) Data acquisition setup.

2.3 Elastic modulus evaluation of the high-strength concrete

2.3.1 Time-dependent concrete's elastic modulus through compression tests

A set of 100 mm × 200 mm concrete cylinders were cast to measure the time-dependent elastic modulus of the high-strength concrete through compression tests. In the field, the prestress force is applied to increase the stiffness of concrete bridge beams and, thereby, their natural frequencies, as shown by the results presented by Saiidi et al. [15]. The PCI beam and all cylindrical specimens were maintained outdoor the laboratory spaces and under the same curing environmental conditions. The elastic modulus E for each cylinder was estimated by the following Eq. (1) in accordance with the ASTM Standards C 469/C 469M–14 [33]:

$$E = E_{fvt} = \frac{\sigma_2 - \sigma_1}{\varepsilon_2 - 0.00005}, \tag{1}$$

where σ_1 and σ_2 are the stress levels corresponding to a longitudinal strain of 0.00005 and the 40% of the ultimate longitudinal compressive stress, respectively. ε_2 is the longitudinal strain produced by σ_2. The aforementioned three values were determined based on graphs depicting longitudinal compressive stress versus longitudinal strain for the individual cylinders, where elastic modulus E was the secant value. One compressometer equipped with two LVDT sensors was used as the strain measurement system. Moreover, the universal testing machine was set at a loading rate of approximately 1 mm/min.

By considering the small second-order effects induced in the PCI beam (Section 2.2), the initial elastic modulus E_{fvt} was determined by Eq. (1) for each cylinder where, conversely, σ_2 was the existing maximum stress in the PCI beam during testing and corresponded to the curing day under observation, as proposed by Bonopera et al. [9]. Similarly, σ_1 was the stress corresponding to a longitudinal strain of 0.00005, whereas ε_2 was the longitudinal strain produced by the maximum stress σ_2. A more realistic investigation of the PCI beam's elastic modulus was thus obtained. A Finite Element (FE) second-order analysis in STRAUS7 environment [34], that assumed nine beam elements and flexural rigidity's variation along the PCI beam based on the parabolic tendon's position (Fig. 1), was used to compute the stress σ_2 during each vibration test by externally applying the corresponding prestress force $N_{0x,\text{aver}}$.

Table 1. Measured unit weight ρ_c, characteristic strength f_{ck}, stresses σ_2, and elastic moduli E and E_{fvt} of the high-strength concrete.

				Eq. (1) with $\sigma_2 = 0.4 f_{ck}$					Eq. (1) with maximum stress σ_2 [9]				
Days of concrete curing	Cyl.	ρ_c (kN/m^3)	f_{ck} (MPa)	σ_2 (MPa)	E (MPa)	E_{aver} (MPa)	E_{ref} (MPa)	Var. (%)	σ_2 (MPa)	E_{fvt} (MPa)	$E_{fvt,\text{aver}}$ (MPa)	$E_{fvt,\text{ref}}$ (MPa)	Var. (%)
28	A	–	85	34	37458	36490	–	–	–	–	–	–	–
28	B	–	94	38	34752				–	–			
28	C	–	93	37	37365				–	–			
28	D	–	83	33	36384				–	–			
66	1	23.68	105	42	39693	37111	37444	+1.7	9	–	40837	41366	+11.9
66	2	24.14	91	36	34528				9	40837			
69	1	24.11	106	42	37294	37341		+2.3	9	41316	40956		+12.2
69	2	24.35	104	42	37387				9	40595			
70	1	24.39	103	41	37931	37880		+3.8	10	43682	42305		+15.9
70	2	24.89	96	38	37828				10	40927			

The measured elastic moduli at 28 days and during the experimental period (Section 2.2) are listed in Table 1 [dataset] [35]. The average elastic moduli E_{aver} and $E_{fvt,\text{aver}}$ were calculated on each required day by testing two cylinders. Vice versa, four specimens were tested at 28 days of curing. The elastic modulus E_{aver} exhibited progressive increments of 1.7%, 2.3%, and 3.8% with respect to the value obtained at 28 days. Conversely, the elastic modulus $E_{fvt,\text{aver}}$ registered progressive increments of 11.9%, 12.2%, and 15.9%, respectively. Thus, the average reference elastic moduli were of E_{ref} = 37,444 MPa and $E_{fvt,\text{ref}}$ = 41,366 MPa. The higher values for $E_{fvt,\text{aver}}$ were caused by the lower values of stresses σ_2 assumed in Eq. (1), as reported in Table 1 [dataset] [35]. The ratio E_{ref} / $E_{fvt,\text{ref}}$ = 37,444 / 41,366 = 0.91 agreed with the ratio for the secant and dynamic elastic modulus of reinforced concrete beams, where the dynamic modulus was determined through transverse vibrations on a set of concrete beam specimens [36]. The mean characteristic strength f_{ck} was of 96 MPa for the compression tests at 66, 69, and 70 days of curing, as detailed in Table 1 [dataset] [35]. The concrete's unit weight, ρ_c = 24.26 kN/m^3, was obtained by the average of the cylinders' weights shown in Table 1 [dataset] [35].

2.3.2 Three-point bending tests

Before the free vibration measurements (Section 2.2), three-point bending tests were performed at 66 days of concrete curing to measure the first-order displacement v at the PCI beam's midspan (i = 5) using two LVDTs labeled L5 in Fig. 4. The recorded average measurement deleted the small rotations along the PCI member's axis. A point load F of 12.5 kN by a transverse steel beam was applied at the PCI beam's midspan (Fig. 2(b)) when the member was axially unloaded ($N_{0x,\mathrm{aver}}$ = 0). The beam was thus preserved without second-order effects. The point load F was pulled both up and down using two hydraulic oil jacks of 1000 kN in force capacity, fixed to the floor, and two additional hydraulic oil jacks of same force capacity fastened to the top of the transverse beam (Fig. 2(b)). The applied force F = 12.5 kN was obtained as the sum of the measurements of the two load cells of 1000 kN in force capacity and 2 mV/V in accuracy, located between the upper oil jacks and two steel plates (Fig. 2(b)). This test was repeated thrice. The midspan displacement measurements v and the load F were recorded for exactly 200 seconds by a data acquisition unit. The average measurement v by the two LVDTs, corresponding to the three repetitions, was of 0.82 mm. Therefore, $E_{\mathrm{static,test}} = FL^3/48vI_{\mathrm{tot,concr}}$ = 37,998 MPa. With respect to the elastic moduli obtained through compression tests (Table 1), the maximum errors were equal to $\Delta_1 = (E_{\mathrm{static,test}} - E_{\mathrm{aver}}) / E_{\mathrm{aver}}$ = (37,998 − 37,111) / 37111 = 2.4% and $\Delta_2 = (E_{\mathrm{static,test}} - E_{fvt,\mathrm{aver}}) / E_{fvt,\mathrm{aver}}$ = (37,998 − 40,837) / 40,837 = –7.0%. The displacements measured by the two reference LVDTs, located at the PCI beam ends (L0 and L10 in Fig. 4), were lower than 0.1 mm in all three repetitions. The PCI beam's supports shown in Fig. 6(a) and 6(b) did not generally allow significant friction phenomena. Given a coefficient of friction μ of 0.1 [37], corresponding to the contact between steel and concrete (Fig. 6(a) and 6(b)), the bending moment at the PCI beam's supports caused by eccentric friction forces $M_\mu = \mu \times \{ [(\rho_s + \rho_c) \times L] / 2 \} \times \mathrm{h} / 2$ = 8.32 kNm did not affect the midspan displacement v and the frequencies obtained by the vibration tests (Section 3.3).

(a)

(b)

Fig. 6. (a) Roller support. (b) Hinge support of the PCI beam.

3. Prestress force effect on fundamental frequency

3.1 Analytical model proposed by Young and Budynas [38]

A simply supported Euler–Bernoulli beam of length L = 14.5 m was used as a reference model for the free vibrations of the PCI beam (Fig. 7). The end constraints of a prestressed concrete bridge beam can be assumed as pinned-end supports [9, 32]. Based on the second-order theory, the prismatic concrete member was subjected to the horizontal prestress force $N_{0x,\text{aver}}$ measured during each test combination (Section 2.2). Specifically, the prestress force $N_{0x,\text{aver}}$ was concentrically assigned to the PCI beam ends without accounting for the geometric eccentricities of the parabolic tendon e_1 and e_2 (Fig. 7). Thus, the prestress force $N_{0x,\text{aver}}$ was assumed to be an externally applied compressive axial force. The deflection shape of the PCI beam's fundamental frequency f_I, in accordance with the first- and second-order theory, is labeled as $v_{I\,\text{mode}}$ in Fig. 7.

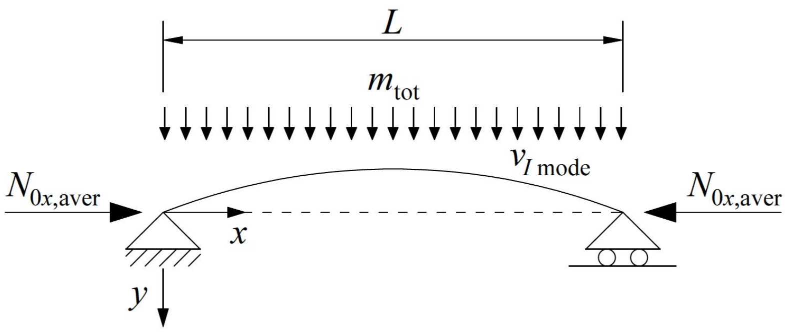

Fig. 7. Reference model for the PCI beam with first mode shape $v_{I\,mode}$. The dashed line represents the PCI beam configuration without any vibrations.

Based on the "*compression-softening*" theory and disregarding the distributed load caused by the parabolic tendon under tensile force, the fundamental frequency f_I of an externally axially loaded simply supported beam (Fig. 7) is as follows [38]:

$$f_I = \frac{\pi}{2}\sqrt{\frac{E\, I_{\mathrm{tot},5-5}\, g}{m_{\mathrm{tot}}\, L^4}}\sqrt{1-\frac{N_{0x,\mathrm{aver}}}{N_{\mathrm{crE}}}}\,, \tag{2}$$

where the PCI beam's weight per unit length is $m_{\mathrm{tot}} = (\rho_s + \rho_c) \times A_{\mathrm{tot}} = 7.601$ kN/m. The elastic modulus on each test day, labeled as E and dependent on the concrete curing, must be assumed in the calculations as the values E_{aver} or $E_{fvt,\mathrm{aver}}$ (Table 1). The cross-sectional second moment of the area of the midspan composite section (concrete and tendon) $I_{\mathrm{tot},5\text{–}5}$ was equal to 2.733×10^{10} mm^4, in accordance with the design. Moreover, the PCI beam's Euler buckling load is given by the formula $N_{\mathrm{crE}} = \pi^2 E I_{\mathrm{tot},5\text{–}5}/L^2$, where the elastic modulus E assumes the values E_{aver} or $E_{fvt,\mathrm{aver}}$ for each test day (Table 2). The gravitational acceleration g was 9.81 m/s^2. Disregarding the term containing the compressive axial force $N_{0x,\mathrm{aver}}$, the fundamental frequency f_I reduces to

$$f_I = \frac{\pi}{2}\left(\frac{E\, I_{\mathrm{tot},5-5}\, g}{m_{\mathrm{tot}}\, L^4}\right)^{1/2}. \tag{3}$$

The dynamic cross-sectional second moment of the area $I_{I,dyn}$ of a concrete bridge beam with parabolic unbonded tendon can be obtained using the corresponding frequency f_I into the first-order Euler–Bernoulli beam model (Eq. (3)) [38]. Therefore, the dynamic cross-sectional second moment of the area $I_{I,dyn}$ of the PCI beam reduces to

$$I_{I,dyn} = \frac{4 f_I^{\,2} m_{\mathrm{tot}}\, L^4}{\pi^2 E_{fvt,\mathrm{aver}}\, g}\,. \tag{4}$$

3.2 Analytical model proposed by Song [30]

The model proposed by Song [30] aims to describe the dynamic behavior of steel bridge beams with parabolic unbonded tendons and pinned-end supports. In particular, the dynamic behavior of the prestressed beam is described by two substructures, which are interconnected through equilibrium and compatibility requirements. In this study, the two reference substructures for the free vibrations of the PCI beam consist of a compressed concrete beam of length $L = 14.5$ m and a tensioned cable of effective length $L_{\mathrm{tendon}} = 14.504$ m (Fig. 8). The behavior of the concrete beam follows the Euler–Bernoulli's assumptions, and the substructures undergo moderate deformations, i.e., large displacements and moderate rotations in order to address the effect of the prestress force $N_{0x,\text{aver}}$ on the dynamic behavior of the member. The effect of the longitudinal vibrations and the rotary inertia are negligible. The PCI beam was subjected to the horizontal prestress force $N_{0x,\text{aver}}$ measured during each test case (Section 2.2). Specifically, the prestress force $N_{0x,\text{aver}}$ was assumed as an internally applied tensile force (Fig. 8).

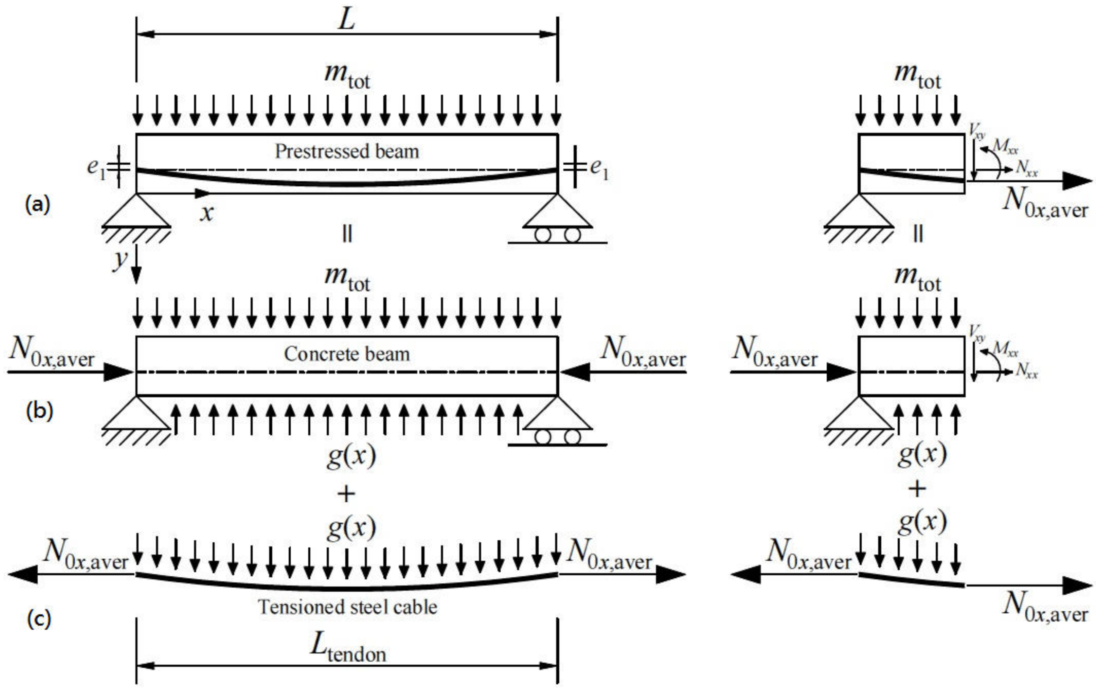

Fig. 8. Substructure layout and internal stress resultants for the PCI beam: (a) prestressed beam, (b) concrete beam, and (c) tensioned steel cable.

By assuming that the concrete beam and the prestressed parabolic tendon interact with the distributed load $g(x)$ under the support of the tendon-held without tangential force (Fig. 8), and disregarding its self-weight, the Galerkin's method was applied to the natural vibration equation of the prestressed member. After some manipulations, the fundamental frequency f_I of an internally axially loaded simply supported prestressed beam (Fig. 8(a)) is as follows [30]:

$$f_I = \sqrt{\frac{E\, I_{\text{tot},5-5}\, \pi^5 + 32\, \lambda f\, L^2}{2\, m_{\text{tot}}\, \pi L^4}}, \tag{5}$$

where the PCI beam's elastic modulus E, dependent on the concrete curing, assumes the values E_{aver} or $E_{fvt,\mathrm{aver}}$ for each test day (Table 2). Vice versa, the term λ containing the tensile axial force $N_{0x,\mathrm{aver}}$ is given by the following formula [30]:

$$\lambda = \frac{E_{\mathrm{tendon}}\ A_{\mathrm{tot,tendon}}}{L_{\mathrm{tendon}}}\left[\frac{16f}{\pi L} - \frac{2L^3}{E\ I_{\mathrm{tot},5-5}\ \pi^3}\left(-m_{\mathrm{tot}} + \frac{8N_{0x,\mathrm{aver}}\ f}{L^2}\right) + \frac{2N_{0x,\mathrm{aver}}\ e_1\ L}{E\ I_{\mathrm{tot},5-5}\ \pi}\right]. \tag{6}$$

3.3 Measurements from free vibration tests

Acceleration time histories at the PCI beam's midspan cross-section with the corresponding Fast Fourier Transforms (FFTs), determined by a block size of 32,768 samples for the three prestress forces $N_{0x,\mathrm{aver}}$, are displayed in Figs. 9, 10, and 11. The Peak Picking Method was adopted. Natural frequencies were located at each peak of the FFTs (Figs. 9(b), 10(b) and 11(b)). Same procedure was used by considering a block size of 16,384 samples. Eighteen of which were totally collected since each vibration test was repeated thrice for every prestress force $N_{0x,\mathrm{aver}}$.

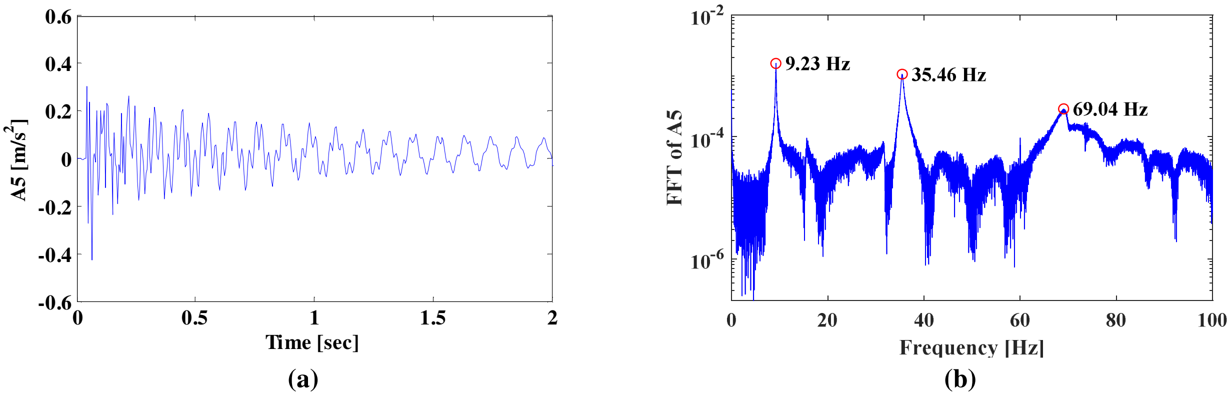

Fig. 9. (a) Acceleration time history for instrumented section A5 when $N_{0x,\mathrm{aver}}$ = 1658 kN. (b) FFT for a block size of 32,768 samples.

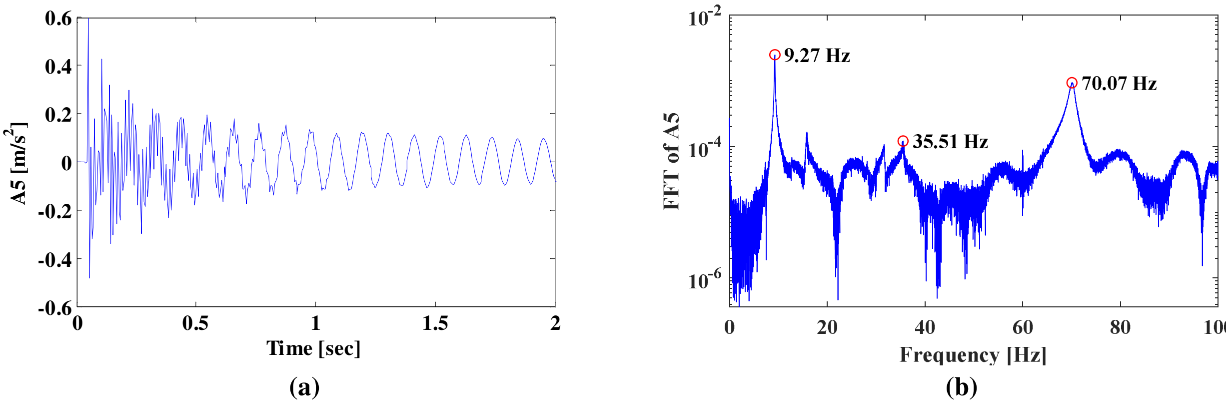

Fig. 10. (a) Acceleration time history for instrumented section A5 when $N_{0x,\mathrm{aver}}$ = 1829 kN. (b) FFT for a block size of 32,768 samples.

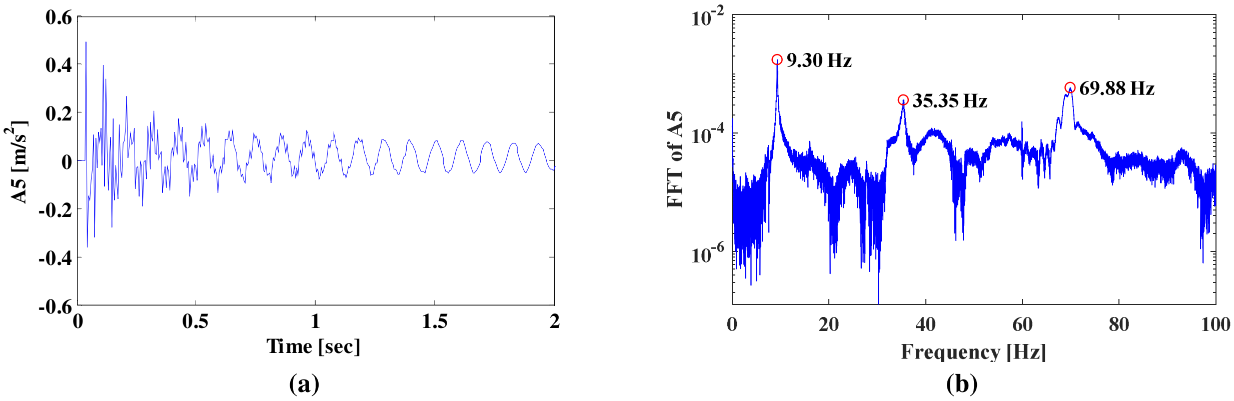

Fig. 11. (a) Acceleration time history for instrumented section A5 when $N_{0x,\text{aver}}$ = 1952 kN. (b) FFT for a block size of 32,768 samples.

The average fundamental frequencies $f_{I,\text{exp}}$, obtained by a block size of 16,384 samples in the FFTs of the three test repetitions, were respectively of 9.20, 9.24 and 9.28 Hz, whereas those obtained by a block size of 32,768 samples were of 9.23, 9.27 and 9.30 Hz. Notably, velocity seismometer A5 on the top of the PCI beam provided identical frequencies $f_{I,\text{exp}}$ in all repetitions. Second- and third-mode frequencies are shown by Peak Picking Method in Figs. 9(b), 10(b), and 11(b). Maximum variation coefficients of 0.1% and 2.2% were respectively obtained in the second- and third-mode frequency evaluations by considering a block size of 16,384 samples in the three repetitions. Maximum variation coefficients of 0.15% and 2.0% were instead achieved by taking into account 32,768 samples. The position of the velocity seismometer A5 at the PCI beam's midspan probably affected the accuracy of the measurements of second-mode frequency. Conversely, proper measurements of third-mode frequency required free vibrations by applying a release force F_d greater than 42.4 kN (Fig. 4). The average measurements of prestress forces N_{0x1} and N_{0x2} for each test case are reported in Table 2 [dataset] [35]. The experimental fundamental frequency $f_{I,\text{exp}}$ increased from 9.20 to 9.28 Hz by considering a block size of 16,384 samples in the FFTs, despite the increase of 17.7% in the average prestress force $N_{0x,\text{aver}}$. The slight increment was confirmed by assuming a block size of 32,768 samples, i.e., increasing the accuracy of the frequency identifications in the FFTs (200 Hz / 32,768 = 0.006 Hz). Specifically, the fundamental frequency $f_{I,\text{exp}}$ increased from 9.23 to 9.30 Hz (Figs. 9(b), 10(b) and 11(b)). Conversely, the elastic modulus E_{aver} increased with time (37,880 / 37,111 = 1.02), corresponding to an increase of 1.1% of the square root of E_{aver} with time. Similarly, the increase of elastic modulus $E_{fvt,\text{aver}}$ with time was 42,305 / 40,837 = 1.04. Therefore, the increase of fundamental frequency is seemingly related to the increasing square root of the concrete's elastic modulus with time. This has confirmed the theoretical results presented by Hamed and Frostig [27], where the natural frequencies of concrete beams with parabolic unbonded tendons were unaffected by prestress force. Additional identification methods have confirmed the estimations provided by Peak Picking Method. Other studies [39, 40] also agree with the aforementioned results reported in Table 2 [dataset] [35].

3.4 Comparison between analytical and experimental fundamental frequencies

Table 2 [dataset] [35] compares the mean values for the experimental fundamental frequency $f_{I,\text{exp}}$ of the PCI beam, obtained using a block size of 32,768 samples in the FFTs, with the corresponding analytical values f_I determined by Eqs. (2), (3) and (5). Elastic moduli E_{aver} and $E_{fvt,\text{aver}}$ were respectively assumed in the three equations. Percentage errors were then obtained by the expression $(f_I - f_{I,\text{exp}}) / f_{I,\text{exp}}$.

Table 2. Comparison between analytical and experimental fundamental frequencies obtained by 32,768 samples in the FFTs.

					f_I with E_{aver}				f_I with $E_{fvt,\text{aver}}$					
Days of concrete curing	N_{0x1} (kN)	N_{0x2} (kN)	$N_{0x,\text{aver}}$ (kN)	$f_{I,\text{exp}}$ (32,768 samples) (Hz)	E_{aver} (MPa)	f_I Eq. (2) [38] (Hz)	f_I Eq. (3) [38] (Hz)	f_I Eq. (5) [30] (Hz)	$E_{fvt,\text{aver}}$ (MPa)	f_I Eq. (2) [38] (Hz)	f_I Eq. (3) [38] (Hz)	f_I Eq. (5) [30] (Hz)	$I_{I,dyn}$ Eq. (4) [38] (mm^4)	f_I STRAUS7 [34] (Hz)
66	1711	1604	1658	9.23	37111	8.40	8.55	8.57	40837	8.83	8.97	8.99	2.7455×10^{10}	9.07
				–		-9.0%	-7.4%	-7.2%		-4.3%	-2.8%	-2.6%	–	-1.7%
69	1887	1770	1829	9.27	37341	8.40	8.57	8.60	40956	8.82	8.98	9.00	2.7454×10^{10}	9.09
				–		-9.4%	-7.6%	-7.2%		-4.9%	-3.1%	-2.9%	–	-1.9%
70	2021	1883	1952	9.30	37880	8.46	8.64	8.66	42305	8.96	9.13	9.15	2.745×10^{10}	9.24
				–		-9.0%	-7.1%	-6.9%		-3.7%	-1.8%	-1.6%	–	-0.6%

The model proposed by Song (Eq. (5)) [30] properly represented the dynamic behavior of the PCI beam with a parabolic unbonded tendon. An average error of −2.4% was gained by considering the elastic modulus $E_{fvt,\text{aver}}$. By assuming a characteristic concrete strength f_{ck} of 96 MPa (Section

2.3.1), the serviceability limit state in the PCI beam was satisfied up to a prestress force $N_{x,SLS,\max}$ of 4300 kN, corresponding to 9.0% of $N_{\mathrm{crE}} = \pi^2 E_{\mathrm{ref}} I_{\mathrm{tot},5\text{–}5}/L^2$ = 48,029 kN. Thus, the maximum applied prestress force during free vibration tests, $N_{0x,\mathrm{aver}}$ = 1952 kN, was 4.1% of N_{crE}. The average error of −7.1% in Table 2 [dataset] [35] was reasonable using the secant elastic modulus E_{aver}, confirming that the elastic modulus $E_{fvt,\mathrm{aver}}$ of PCI beams differs from the secant E_{aver} during vibrations and when small second-order effects are applied [9, 36]. Table 2 also shows that the errors slightly increased by assuming the model proposed by Young and Budynas [38]. In fact, an average error of −2.6% was obtained by the first-order beam model (Eq. (3)) and considering the elastic modulus $E_{fvt,\mathrm{aver}}$, even though the second-order effects in the PCI beam were between 3.5% and 4.1% of N_{crE}. Notably, the second-order beam model (Eq. (2)) exhibited a constant course of frequency f_I because the decrease predicted by the "*compression-softening*" model was cancelled out by the increase of elastic moduli E_{aver} and $E_{fvt,\mathrm{aver}}$ with time.

A FE first-order analysis in STRAUS7 environment [34], assuming a discretization of the PCI beam in nine beam elements, indicated that the frequency f_I does not significantly vary with respect to the model proposed by Song (Eq. (5)). Furthermore, an average error of −1.4% was gained by the comparison with the mean experimental frequencies $f_{I,\mathrm{exp}}$ in Table 2. More specifically, the initial elastic moduli $E_{fvt,\mathrm{aver}}$ and the values of cross-sectional second moment of the area $I_{I,dyn}$ for each test day, obtained by Eq. (4) and considering the corresponding frequency f_I (Eq. (5)), were accounted for (Table 2). Notably, the values of dynamic cross-sectional second moment of the area $I_{I,dyn}$ of the PCI beam (Table 2) increased by an average value of 0.5% when compared with the original cross-sectional second moment of the area $I_{\mathrm{tot},5\text{–}5}$ (the midspan cross-section). Conversely, the values $I_{I,dyn}$ did not vary, i.e., from 2.7455×10^{10} to 2.745×10^{10} mm^4, despite the increase of 17.7% in prestress force $N_{0x,\mathrm{aver}}$ (Table 2). This deduces that the stiffness effect in concrete bridge beams with parabolic unbonded tendons is null because of the softening effect caused by the increase in compressive (prestress) force.

An additional FE first-order analysis in STRAUS7 [34] was finally used to examine the eccentric mass of 1.05 kN composed of load cell, steel transition part, and steel plate (Fig. 3(a)) at the PCI beam ends, for a corresponding value equal to 1.9% of its weight. Similarly to the numerical simulations reported in Bonopera et al. [9], the fundamental frequency did not vary with respect to that obtained by the refence model, i.e., Eq. (5). When the mass of load cells and/or stressing jacks are greater than the weight of the tested specimens, as occurred in the experiments of Noble et al. [1], fundamental frequencies are affected by a maximum error of approximately 6%.

4. Conclusions

A testing program was conducted on a large-scale PCI beam made of high-strength concrete to study the variation of fundamental frequency in concrete bridge beams with parabolic unbonded tendons, where second-order effects are lower than 10% of N_{crE}. A small range of second-order effects, i.e., lower than 4.5% of N_{crE}, were induced to prevent cracking phenomena during testing. This work supplements the limited laboratory tests on large-scale prestressed concrete beams because of the difficult task of performing such experiments with and without prestress force. Within the limitations of the research and the results obtained, the following conclusions are drawn regarding concrete bridge beams with parabolic unbonded tendons:

1. The initial concrete elastic modulus $E_{fvt,\mathrm{aver}}$ should be considered when simulating free vibrations in a numerical analysis, because the maximum stress due to vibrations is much lower than the 40% of f_{ck}, as proposed by Bonopera et al. [9]. Notably, the initial elastic modulus $E_{fvt,\mathrm{aver}}$ could be obtainable by the ratio E_{ref} / $E_{fvt,\mathrm{ref}}$ = 0.91, where the secant modulus E_{ref} can be determined by compression tests (Eq. (1)).
2. The fundamental frequency is unaffected by prestress force. A small variation in frequency of 0.8% was recorded despite the increment of prestress force of 17.7%. This was theoretically demonstrated by Hamed and Frostig [27], and confirmed by the large-scale experiments presented.

3. The fundamental frequency is sensitive to variations in the square root of the concrete's elastic modulus during the early curing process, as observed for concrete bridge beams with straight unbonded tendons in Bonopera et al. [9]. A small increment in frequency of 0.8% (Point 2) was registered in relation to the variation of secant and initial elastic moduli E_{aver} and $E_{fvt,\mathrm{aver}}$ of 2.1% and 3.6%, respectively.
4. The relationship between prestress force and fundamental frequency is well approximated by the model proposed by Song [30] that describes the behavior of a bridge beam as a combination of two substructures interconnected, i.e., a compressed beam and a tensioned parabolic cable. An average error of −2.4% was determined by comparing the analytical and the experimental frequencies (Table 2 [dataset] [35]).
5. The tensioned parabolic tendon increases slightly the concrete beam's stiffness (and natural frequency) without prestress force but, vice versa, the corresponding non-increase in stiffness (and natural frequency) with increasing prestress force is caused by the combination of stiffening and softening effects. In the PCI beam, the slight increment of experimental frequency (Point 2) was caused by variation in the square root of the concrete's elastic modulus. The increase of PCI beam's stiffness based on the tendon eccentricity may also have affected this trend [25, 42].
6. Conversely, the prominent increase of natural frequencies (and stiffness) with increasing prestress force, as reported in [14–18], may be caused by microcrack closure under the high prestress forces [23–25]. In fact, second-order effects greater than 10% of N_{crE} were induced in the concrete beam specimens.
7. Another study [41] attempted to use natural frequencies as indicators predicting prestress loss in a concrete bridge, where second-order effects were of approximately 6.6% with respect to the first-order theory. Nonetheless, frequency has been confirmed to be an unsuitable indicator for prestress loss detection, as declared by Saiidi et al. [15], Jaiswal [25],

and Bonopera et al. [9]. In fact, because of the reasons above mentioned, frequency remains relatively constant when changes in prestress force are induced.

8. Consequently, further studies are intended for improving a static NDT method [8] for predicting prestress losses in concrete bridges.

Acknowledgments

Experiments were conducted at the National Center for Research on Earthquake Engineering (NCREE) and supported by a grant from the National Applied Research Laboratories (NCREE–06105C1005). M.B. acknowledges the financial support provided by the Ministry of Science and Technology of Taiwan (MOST 105-2811-E-492-001). N.T. acknowledges the financial support of the "Research Program FAR 2019" provided by the University of Ferrara. A special gratitude is extended to the technicians of NCREE and students of National Taiwan University, who provided considerable assistance to the authors.

References

1. D. Noble, M. Nogal, A. O'Connor, V. Pakrashi, Dynamic impact testing on post–tensioned steel rectangular hollow sections; An investigation into the "compression–softening" effect, J. Sound Vib. 355 (2015) 246–63.
2. D. Noble, M. Nogal, A. O'Connor, V. Pakrashi, The effect of prestress force magnitude and eccentricity on the natural bending frequencies of uncracked prestressed concrete beams, J. Sound Vib. 365 (2016) 22–44.
3. A. Miyamoto, K. Tei, H. Nakamura, J.W. Bull, Behavior of pre–stressed beam strengthened with external tendons, J. Struct. Eng. 126 (9) (2000) 1033–44.
4. S.S. Law, Z.R. Lu, Time domain responses of a pre–stressed beam and pre–stress identification, J. Sound Vib. 288 (4–5) (2005) 1011–25.
5. Z.R. Lu, S.S. Law, Identification of pre–stress force from measured structural responses, Mech. Syst. Signal Process 20 (8) (2006) 2186–99.

6. M. Bonopera, K.C. Chang, C.C. Chen, T.K. Lin, N. Tullini, Compressive column load identification in steel space frames using second–order deflection–based methods, Int. J. Struct. Stab. Dy. 18 (7) (2018a) 1–16 art. ID 1850092.
7. M. Bonopera, K.C. Chang, C.C. Chen, Z.K. Lee, N. Tullini, Axial load detection in compressed steel beams using FBG–DSM sensors, Smart Struct. Syst. 21 (1) (2018b) 53–64.
8. M. Bonopera, K.C. Chang, C.C. Chen, Y.C. Sung, N. Tullini, Feasibility study of prestress force prediction for concrete beams using second–order deflections, Int. J. Struct. Stab. Dy. 18 (10) (2018c) 1–19 art. ID 1850124.
9. M. Bonopera, K.C. Chang, C.C. Chen, Y.C. Sung, N. Tullini, Prestress force effect on fundamental frequency and deflection shape of PCI beams, Struct. Eng. Mech. 67 (3) (2018d) 255–265.
10. M. Bonopera, K.C. Chang, C.C. Chen, T.K. Lin, N. Tullini, Bending tests for the structural safety assessment of space truss members, Int. J. Space Struct. 33 (3–4) (2018e) 138–149.
11. N. Tullini, F. Laudiero, Dynamic identification of beam axial loads using one flexural mode shape, J. Sound Vib. 318 (1–2) (2008) 131–47.
12. N. Tullini, G. Rebecchi, F. Laudiero, Bending tests to estimate the axial force in tie–rods, Mech. Res. Commun. 44 (2012) 57–64.
13. T.H. Wang, R. Huang, T.W. Wang, The variation of flexural rigidity for post–tensioned prestressed concrete beams, J. Mar. Sci. Technol. 21 (3) (2013) 300–8.
14. T. Hop, The effect of degree of prestressing and age of concrete beams on frequency and damping of their free vibration, Mater. Struct. 24 (1991) 210–20.
15. M. Saiidi, B. Douglas, S. Feng, Prestress force effect on vibration frequency of concrete bridges, J. Struct. Eng. 120 (7) (1994) 2233–41.
16. J.T. Kim, C.B. Yun, Y.S. Ryu, H.M. Cho, Identification of prestress–loss in PSC beams using modal information, Struct. Eng. Mech. 17 (3–4) (2004) 467–82.

17. Y. Zhang, R. Li, Natural frequency of full–prestressed concrete beam, Transactions Tianjin Univ. 13 (5) (2007) 354–59.
18. J. Li, F. Zhang, Experimental research and numerical simulation of influence of pre-stress values on the natural vibration frequency of concrete simply supported beams, J. Vibroeng. 18 (7) (2016) 4592–604.
19. G. Rebecchi, N. Tullini, F. Laudiero, Estimate of the axial force in slender beams with unknown boundary conditions using one flexural mode shape, J. Sound Vib. 332 (18) (2013) 4122–35.
20. T. Kernicky, M. Whelan, E. Al-Shaer, Dynamic identification of axial force and boundary restraints in tie rods and cables with uncertainty quantification using Set Inversion Via Interval Analysis, J. Sound Vib. 423 (2018) 401–20.
21. N. Tullini, G. Rebecchi, F. Laudiero, Reliability of the tensile force identification in ancient tie-rods using one flexural mode shape, Int. J. Archit. Herit. 13 (3) (2019) 402–10.
22. Y. Toyota, T. Hirose, S. Ono, K. Shidara, Experimental study on vibration characteristics of prestressed concrete beam, Procedia Eng. 171 (2017) 1165–72.
23. G. Deák, Discussion on prestress force effect on vibration frequency of concrete bridges, J. Struct. Eng. (1996) 458–9.
24. S.K. Jain, S.C. Goel, Discussion on prestress force effect on vibration frequency of concrete bridges, J. Struct. Eng. (1996) 459–60.
25. O.R. Jaiswal, Effect of prestressing on the first flexural natural frequency of beams, Struct. Eng. Mech. 28 (5) (2008) 515–24.
26. M.H. Noh, T.R. Seong, J. Lee, K.S. Park, Experimental investigation of dynamic behavior of prestressed girders with internal tendons, Int. J. Steel Struct. 15 (2) (2015) 401–14.
27. E. Hamed, Y. Frostig, Natural frequencies of bonded and unbonded pre–stressed beams pre–stress force effects, J. Sound Vib. 295 (1–2) (2006) 28–39.

28. J. T. Kim, Y. S. Ryu and C. B. Yun, Vibration based method to detect pre–stress loss in beam type bridges, Smart Syst. Non-destr. Eval. Civil Infrastr., V. 5057 of Proceedings of SPIE (2003) 559–568.
29. N.F. Ortega, J.M. Moro, R.S. Meneses, Theoretical model to determine bond loss in prestressed concrete with reinforcement corrosion, Struct. Eng. Mech. 65 (1) (2018) 1–7.
30. Y. Song, Dynamics of Highway Bridges, Beijing: China Communications Press, China, Chapter 1, 113–20, 2000 (in Chinese).
31. ACI 318–14, Building Code Requirements for Structural Concrete and Commentary, American Concrete Institute, Farmington Hills, MI, 2014.
32. M. Bonopera, K.C. Chang, C.C. Chen, Z.K. Lee, Y.C. Sung, N. Tullini, Fiber Bragg grating–differential settlement measurement system for bridge displacement monitoring: Case study, J. Bridge Eng. (2019). Article in Press.
33. Annual Book of ASTM Standards, Section 4: Construction vol. 04.02. Concrete & aggregates, American Society for Testing & Materials, 2016.
34. STRAUS7. Release 2.3.3. G+D Computing Pty Ltd. Copyright 2004.
35. [dataset] K.C. Chang, Experimental study on the fundamental frequency of prestressed concrete bridge beams with parabolic unbonded tendons, National Center for Research on Earthquake Engineering, Experiment Data Center, 2018. https://www.ncree.org/expdb/PrjInfo.aspx?pid=NCREE-R2016501.
36. S. Jerath, M.M. Shibani, Dynamic modulus for reinforced concrete beams, J. Struct. Eng. 110 (6) (1984) 1405–10.
37. BS EN 12812:2008, Falsework – Performance requirements and general design, British Standards Institution, 2008.
38. W.C. Young, R.G. Budynas, Roark's Formulas for Stress and Strain, McGraw–Hill, Chapter 16, 767–68, 2002.

39. S. Jacobs, G. De Roeck, Dynamic testing of a pre–stressed concrete beam, In: 6th National Congress on Theoretical and Applied Mechanics, 2003.

40. M.P. Limongelli, D. Siegert, E. Merliot, J. Waeytens, F. Bourquin, R. Vidal, V. Le Corvec, I. Gueguen, L.M. Cottineau, Damage detection in a post tensioned concrete beam – Experimental investigation, Eng. Struct. 128 (2016) 15–25.

41. M. Kato, S. Shimada, Vibration of PC bridges during failure process, J. Struct. Div. 112 (7) (1986) 1692–1703.

42. Y. Wang, Research on fundamental frequencies and dynamic characteristics of pre-stressed concrete beams based on experiment and numerical simulation, Mechanika 23 (4) (2017) 552–61.